Received: 23 April 2020 | Revised: 9 July 2020 | Accepted: 27 July 2020

DOI: 10.1002/humu.24089

RESEARCH ARTICLE

Human Mutation HGVS HUMAN GENOME VARIATION SOCIETY WILEY

Functional consequences of *SLC1A3* mutations associated with episodic ataxia 6

Aparna S. Chivukula | Mariia Suslova | Daniel Kortzak | Peter Kovermann | Christoph Fahlke

Institute of Biological Information Processing, Molekular- und Zellphysiologie (IBI-1) Forschungszentrum Jülich, Jülich, Germany

Correspondence
Peter Kovermann and Christoph Fahlke, Institute of Biological Information Processing, Molekular- und Zellphysiologie (IBI-1) Forschungszentrum Jülich, 52428 Jülich, Germany.
Email: p.kovermann@fz-juelich.de (P. K.) and c.fahlke@fz-juelich.de (C. F.)

Funding information
Bundesministerium für Bildung und Forschung, Grant/Award Number: BMBF 01GM1907C

Abstract

The episodic ataxias (EA) are a group of inherited neurological diseases characterized by paroxysmal cerebellar incoordination. There exist nine forms of episodic ataxia with distinct neurological symptoms and genetic origins. Episodic ataxia type 6 (EA6) differs from other EA forms in long attack duration, epilepsy and absent myokymia, nystagmus, and tinnitus. It has been described in seven families, and mutations in *SLC1A3*, the gene encoding the glial glutamate transporter EAAT1, were reported in each family. How these mutations affect EAAT1 expression, subcellular localization, and function, and how such alterations result in the complex neurological phenotype of EA6 is insufficiently understood. We here compare the functional consequences of all currently known mutations by heterologous expression in mammalian cells, biochemistry, confocal imaging, and whole-cell patch clamp recordings of EAAT1 transport and anion currents. We observed impairments of multiple EAAT1 properties ranging from changes in transport function, impaired trafficking to increased protein expression. Many mutations caused only slight changes illustrating how sensitively the cerebellum reacts on impaired EAAT1 functions.

KEYWORDS
anion currents, EAAT1, episodic ataxia, gain-of-function, glutamate transporter

1 | INTRODUCTION

Episodic ataxias (EAs) are rare neurological conditions with episodes of recurrent incoordination and truncal instability as common features (Jen et al., 2007). Most of the patients suffer from additional neurological symptoms, such as epilepsy, dystonia, and migraine-like headache. Based on such additional neurological symptoms as well as on genetic origin nine variants of autosomal dominant EAs (EA1 to 9) have been distinguished (Cader, Steckley, Dyment, McLachlan, & Ebers, 2005; Conroy et al., 2014; Damji et al., 1996; Kerber, Jen, Lee, Nelson, & Baloh, 2007; Ophoff et al., 1996; Piarroux et al., 2020). EA1 and EA2 are the most common and best characterized forms of episodic ataxia. EA1 is caused by mutations in *KCNA1*, and affected patients suffer from brief periods of dizziness and imbalance. Mutations in *CACNA1A* cause EA2, with incoordination, vertigo and slurring of speech as typical symptoms, disease onsets in infancy and early childhood, and episodes lasting hours to days. EA5 and EA8 were linked to mutations in genes encoding cytoskeletal components

Peter Kovermann and Christoph Fahlke contributed equally to this work.

such as ubiquitin-protein ligase 4, and mutations in the fibroblast growth factor 14 have been recently associated to the newly defined subtype EA9. So far, causal genes have not yet been identified for EA3, 4, and 7. There are other EA syndromes that have been associated to mutations in the ion channel genes *KCNA2* and *SCN2A* (Corbett et al., 2016; Maksemous, Smith, Sutherland, Sampaio, & Griffiths, 2018; Schwarz et al., 2016, 2019), but thus far they have not been designated as specific EA-subtypes.

Episodic ataxia type 6 (EA6) combines paroxysmal cerebellar incoordination with epilepsy and migraine-like headache and differs from other EA forms in the occurrence of long-lasting attacks of ataxia and epilepsy and absent myokymia, nystagmus, and tinnitus (Jen et al., 2007). Thus far, EA6 has been reported in only seven families, and was associated with mutations in *SLC1A3*, encoding the glial excitatory amino acid transporter 1 (EAAT1), in all the cases (Figure 1; Choi, Jen, et al., 2017; Choi, Kim, et al., 2017;

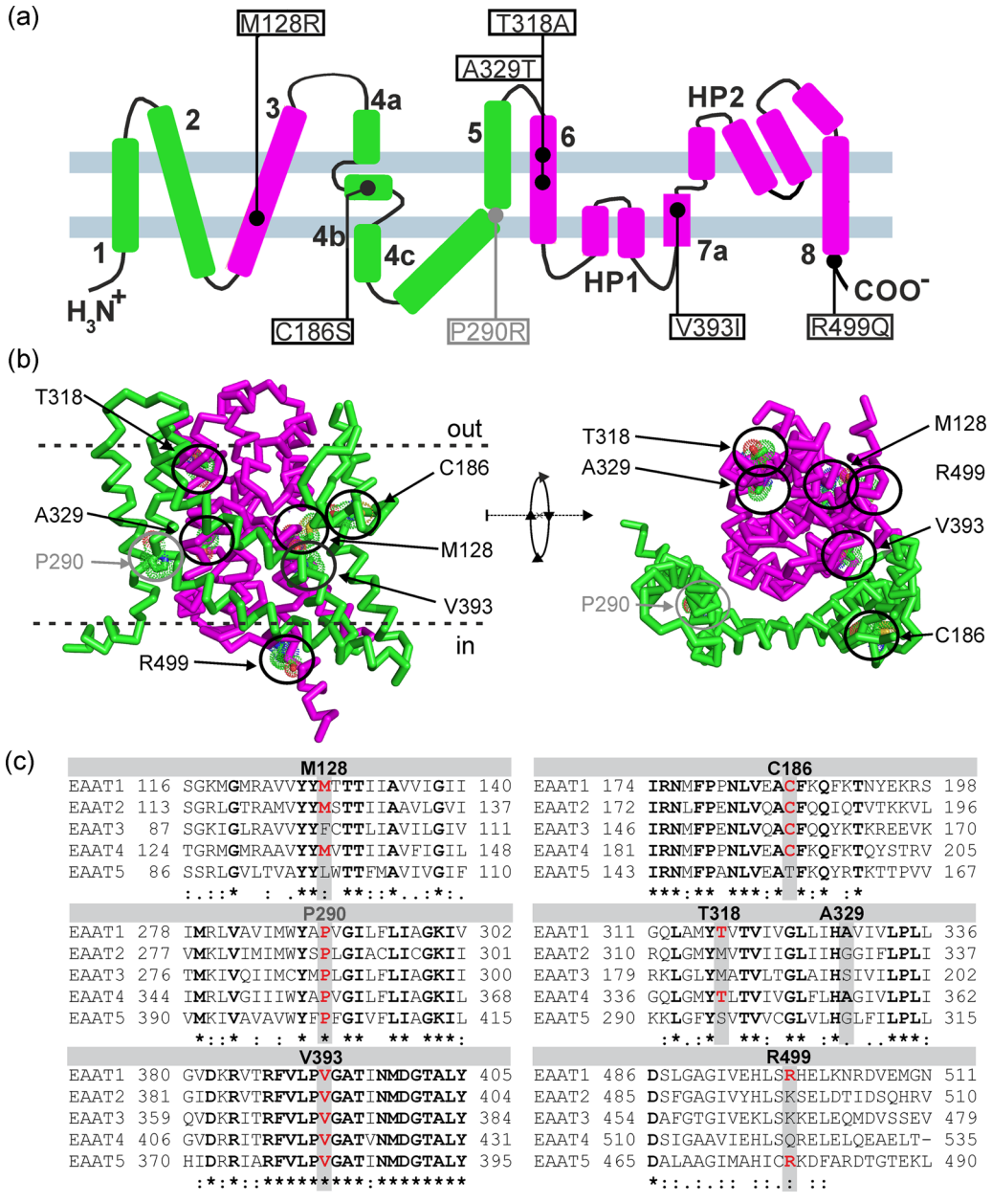

FIGURE 1 Localizations of EA6-associated mutations in *h*EAAT1. (a) Membrane topology of *h*EAAT1 shows the spatial distribution of EA6-associated missense mutations within the protein (p.M128R (NM_004172.4: c.383T>G), p.C186S (NM_004172.4: c.556T>A), p.P290R (NM_001166695.1: c.869C>G), p.T318A (NM_004172.4: c.952A>G), p.A329T (NM_004172.4: c.985G>A), p.V393I (NM_004172.4: c.1177G>A), p.R499Q (p.R454Q (XM_024446182.1: c.1361G>A)). (b) The positions of the newly identified EA6 mutations in the tertiary structure of *h*EAAT1 (colors: green: trimerization domain, magenta: transport domain). The crystal structure of EAAT1 in complex with L-aspartate (pdb ID: 5LLM, Canul-Tec et al., 2017) was used as template. (c) Alignments of human EAAT isoform sequences for 6–12 amino acids next to the disease-associated amino acid exchanges. EAAT1, excitatory amino acid transporter 1

de Vries et al., 2009; Iwama et al., 2017; Jen, Wan, Palos, Howard, & Baloh, 2005; Pyle et al., 2015).

The first reported case of EA6 was a 10-year-old boy who suffered from severe episodes of ataxia, epileptic seizures, and hemiplegia during his childhood (Jen et al., 2005). He carries a heterozygous *SLC1A3* missense mutation (RefSeq NM_001166695.1: c.869C>G: p.Pro290Arg) predicting a proline-to-arginine replacement in transmembrane domain 5 (p.P290R) of the human EAAT1 (Jen et al., 2005). EAATs function as both secondary-active glutamate transporters and anion channels (Fahlke, Kortzak, & Machtens, 2016), and we demonstrated that the P290R substitution impairs glutamate transport, but causes gain-of-function of EAAT1 anion channels (Hotzy, Schneider, Kovermann, & Fahlke, 2013; Winter, Kovermann, & Fahlke, 2012). To understand how increased EAAT1 anion currents cause ataxia in EA6 we generated a transgenic mouse model—the *Slc1a3*$^{P290R/+}$ mouse—and demonstrated that excessive chloride efflux in the second postnatal week results in Bergmann glia apoptosis and cerebellar atrophy (Kovermann et al., 2020).

Here, we study the functional consequences of the remaining six known EA6-associated *SLC1A3* mutations using heterologous expression in mammalian cells, confocal imaging, biochemistry, and whole-cell patch clamping. A mutation predicting p.M128R (Ref Seq NM_004172.4: c.383T>G: p.Met128Arg) was reported in a 10-year-old girl with disease onset at 11 months and episodes of truncal ataxia and strabismus (Iwama et al., 2017). In another family, three patients, who experienced ataxia episodes associated with nausea, photophobia, vertigo, and speech and vision problems from early childhood, and one unaffected family member carry a *SLC1A3* mutation causing the p.C186S (RefSeq NM_004172.4: c.556T>A: p.Cys186Ser) substitution (de Vries et al., 2009). Choi et al. reported a p.V393I mutation (RefSeq NM_004172.4: c.1177G>A: p.Val393Ile) in two unaffected and two affected members of one family, who suffered from unsteadiness and dizziness with a late onset at age 55 years (Choi, Jen, et al., 2017; Choi, Kim, et al., 2017). A *SLC1A3* mutation resulting in expression of p.T318A *h*EAAT1 (RefSeq NM_004172.4: c.952A>G: p.Thr318Ala) was reported in patients with ataxia, dizziness, and dysarthria, and the p.A329T mutation (RefSeq NM_004172.4: c.985G>A: p.Ala329Thr) was found in a patient carrying additional *CACNA1A* mutations and suffering from ataxia, dizziness, and epileptic seizures (Choi, Kim, et al., 2017). Exome sequencing in undiagnosed inherited ataxias identified the p.R499Q mutation as p.R454Q (RefSeq XM_024446182.1: c.1361G>A: p.Arg454Gln) in a transcript variant of *h*EAAT1 (isoform X2) in patients reporting speech disturbances and upper limb clumsiness (Pyle et al., 2015).

EAATs are trimeric proteins with three subunits associating via immobile trimerization domains (Figure 1). They are prototypical elevator transporter: each subunit exhibits a mobile transport domain that contains all substrate-binding sites and that shuttle substrates from outside to inside or vice versa via combined 16 Å vertical movement and 37° rotation (Reyes, Ginter, & Boudker, 2009). Whereas the p.P290R and p.C186S exchange amino acids within the trimerization domain (de Vries et al., 2009; Jen et al., 2005), all other known mutations are localized in the transport domain (Figure 1a,b; Canul-Tec et al., 2017). Figure 1c demonstrates the conservation of affected residues within human EAATs.

2 | METHODS

2.1 | Heterologous expression of *h*EAAT1

The coding region of human EAAT1 (kindly provided by Dr. S. Amara, National Institute of Mental Health, Bethesda) was subcloned into pcDNA3.1 and carboxy terminally linked to the coding region of the yellow fluorescent protein using PCR-based strategies. Point mutations in human EAAT1 (p.M128R: RefSeq NM_004172.4: c.383T>G: p.Met129Arg; p.C186S: RefSeq NM_004172.4: c.556T>A: p.Cys186Ser; p.T318A: RefSeq NM_004172.4: c.952A>G: p.Thr318Ala; p.A329T: RefSeq NM_004172.4: c.985G>A: RefSeq p.Ala329Thr; p.V393I: RefSeq NM_004172.4: c.1177G>A: p.Val393Ile; p. R499Q [R454Q]: RefSeq XM_024446182.1: c.1361G>A: Arg499Gln [Arg454Gln]) were generated by polymerase chain reaction (PCR)-based techniques as described (Winter et al., 2012). For transient transfection of HEK293T cells, we used the $Ca_3(PO_4)_2$ technique as described (Garcia-Olivares et al., 2008). Coexpression of WT *h*EAAT1–YFP with p.T318A *h*EAAT1–YFP, p.M128R *h*EAAT1–YFP, and untagged pcDNA3.1 wild type (WT) *h*EAAT1 with pcDNA3.1 YFP were performed by transfecting HEK293T cells with a DNA ratio of 1:1. In some of our experiments pcDNA3.1 p.E281Q *h*ClC-4 encoding the human Cl^-/H^+ exchanger 4 carrying the E281Q substitution (NM_001830.4: c:841G>C) and carboxy-terminally linked to the coding sequence for mCherry (Guzman, Grieschat, Fahlke, & Alekov, 2013) was cotransfected with pcDNA3.1 WT *h*EAAT1–YFP.

2.2 | Confocal microscopy and biochemistry

For confocal imaging HEK293T cells expressing WT or mutant *h*EAAT1–YFP fusion proteins were plated on Poly L-Lysine coated coverslips 24 hr after transfection. Images were acquired with a Carl-Zeiss LSM 780 inverted microscope (Jena, Germany) using a ×63 /1.40 NA oil immersion objective in PBS at room temperature 48 hr after transfection. YFP was excited with an argon laser (488 nm), and emission was detected between 543–594 nm. Images were analyzed with Fiji image analysis software (NIH). Transfection rates of WT and mutant EAAT1 were estimated as ratios of transfected cells by the total number of seeded cells in three independent transfections (Figure 2c). Each transfection was seeded on two cover slips, and ratios were calculated from cell counts of 5–7 randomly selected region of interests on each coverslip (n = 5,052/7,589/5,379/5,195/6,367/3,311/2,784 cells; WT/p.M128R/p.C186S/p.T318A/p.A329T/p.V393I/.R499Q).

For sodium dodecyl sulfate (SDS)-polyacrylamide gel electrophoresis (PAGE), cells were split 12 hr after transfection in 5 cm

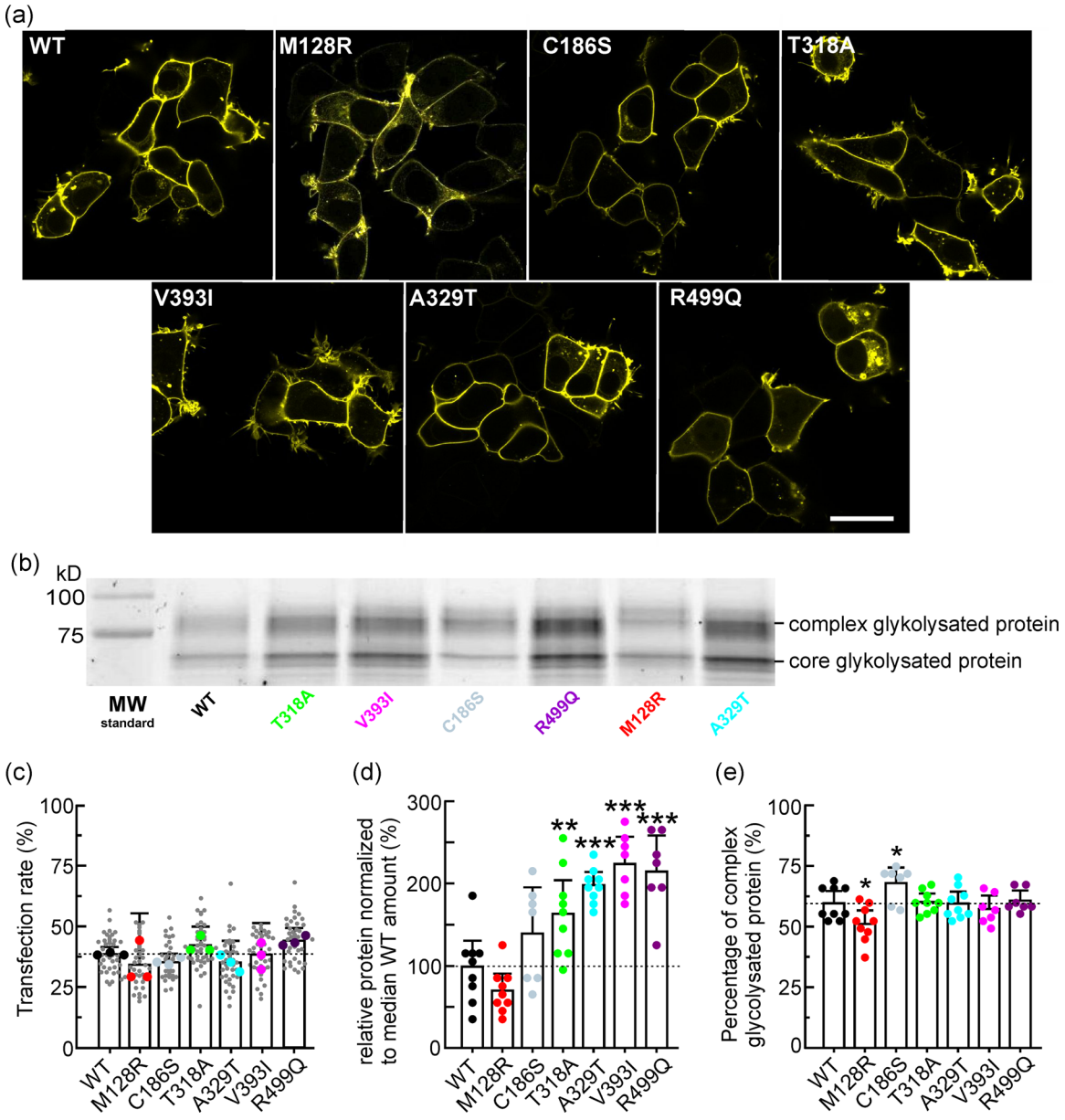

FIGURE 2 Membrane insertion and relative protein expression of WT and mutant *h*EAAT1 variants. (a) Representative confocal microscopy images of HEK293T cells transiently transfected with WT and mutant *h*EAAT1–YFP variants (scale bar = 25 μm). (b) sodium dodecyl sulfate-polyacrylamide gel electrophoresis of HEK293T cells lysates expressing WT or mutant *h*EAAT1–YFP. (c) Bar graphs showing the transfection rates for each tested EAAT1 variant. Big dots represent mean values for each independent transfection, and small dots show single values obtained in all tested region of interests. (d) and (e), Statistical analysis of relative protein amounts for total protein (d) and complex glycosylated fractions (e). Each point represents one individual transfection. Data were analyzed with one-way analysis of variance and Holm-Sidak post hoc testing. Data represent mean values ± 95% CI. EAAT1, excitatory amino acid transporter 1; WT, wild type

tissue culture dishes. After 48 hr, the cells were centrifuged twice at 4°C (10′/4,500 rpm and 30′/13,000 rpm) followed by resuspension and incubation on ice. After solubilization in 0.4% dodecyl-maltoside for 30′ on ice, lysates were centrifuged again (35′/13,000 rpm at 4°C). The concentration of the protein in the supernatant was determined with the BCA protein assay kit (Abcam, ab102536). Expression levels and glycosylation states were estimated by scanning 10% SDS-PAGEs loaded with 15 μg protein from cell lysate of HEK293T cells expressing *h*EAAT1–YFP fusion proteins with a gel scanner (Typhoon FLA9500, GE Healthcare, Sweden) using the Fiji gel analysis plug-in. Protein expression levels (Figures 3d, 4d, and 5d) were determined by multiplying relative total protein amounts (Figure 2d) and percentages of complex glycolysated proteins (Figure 2e).

2.3 | Electrophysiology

Whole-cell patch-clamp recordings were performed using an EPC-10 amplifier controlled by PatchMaster software (HEKA

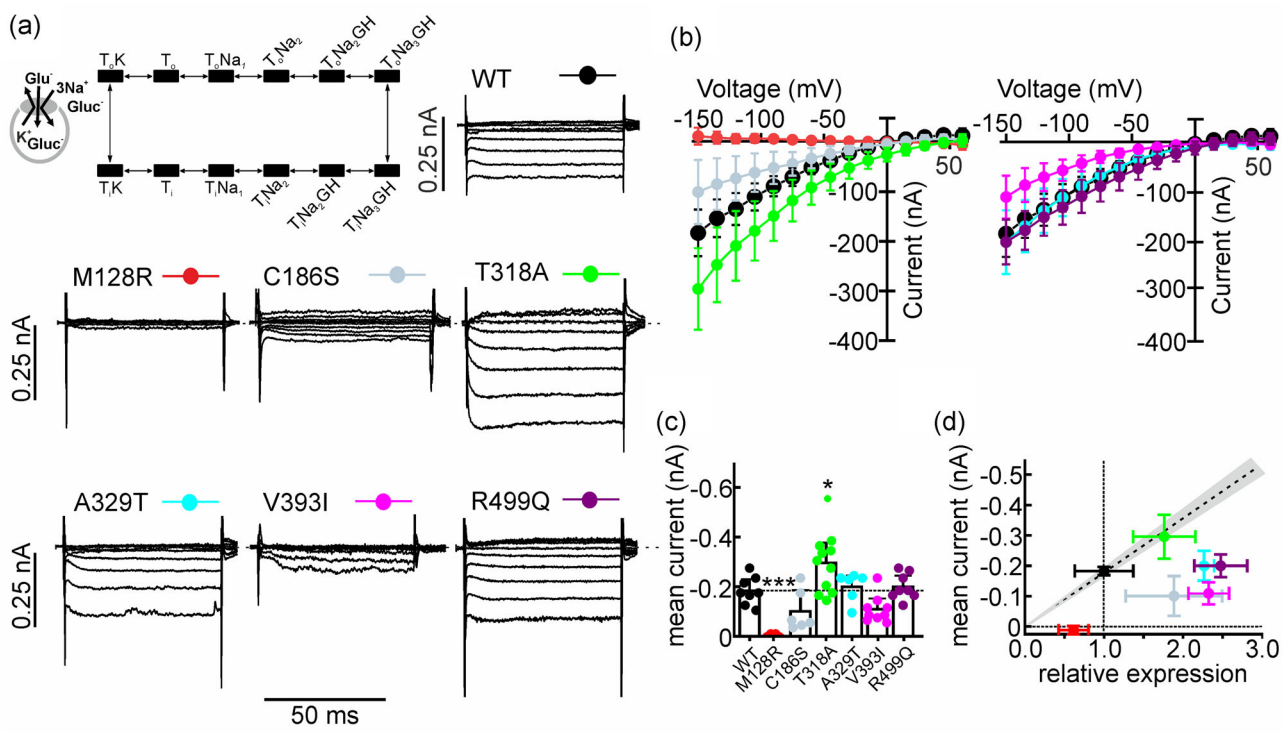

FIGURE 3 Glutamate uptake currents of WT and mutant *h*EAAT1 variants. (a) Representative uptake currents for WT or EA6-associated *h*EAAT1 missense variants. Glutamate uptake currents were calculated by subtracting whole-cell currents before and after application of 0.5 mM L-glutamate in the bath solution. The inset shows the ionic conditions during the experiment and the conformational states, which can be assumed by the transporter. (b) Current-voltage relationships of glutamate uptake currents from WT and mutant *h*EAAT1 variants. Current amplitudes were measured 50 ms after the voltage jump. (c) Uptake current amplitudes at −150 mV for WT and mutant *h*EAAT1. (d) Plot of uptake currents at −150 mV vs. relative expression levels obtained in biochemical experiments. The dashed line connects the origin of the plot with mean current amplitudes/relative expression levels of WT *h*EAAT1 and permits prediction of WT current amplitudes at different expression levels. Data were analyzed with *one-way* ANOVA and Holm-Sidak post hoc testing. Data in (b)–(d) are provided as mean values ± 95% CI. Dots in (c) represent values obtained from individual cells. EAAT1, excitatory amino acid transporter 1; WT, wild type

Elektronik) or an Axon 200 A amplifier controlled by Clampex 10.5 software (Molecular Devices) on Day 2 after transfection. Borosilicate pipettes (Harvard Apparatus) were pulled with resistances of 1.5–2.5 MΩ, and voltage errors were adjusted to less than 5 mV with series resistance compensation when necessary. Currents were filtered at 10 kHz and digitized with a sampling rate of 50 kHz using the built-in AD/DA converter of the amplifier (HEKA Elektronik) or an external Axon 1550 A device (Molecular Devices). Standard external solutions for measuring *h*EAAT1 anion currents contained (in mM): 140 $NaNO_3$, 10 4-(2-hydroxyethyl)-1-piperazineethanesulfonic acid (HEPES), 4 KCl, 2 $CaCl_2$, 1 $MgCl_2$, ±0.5 L-glutamate, pH 7.4. Standard internal solutions contained 115 KNO_3 ($NaNO_3$), 10 HEPES, 2 $MgCl_2$, 5 EGTA, pH 7.4. To measure glutamate transport currents, NO_3 was equimolarly substituted with gluconate in internal and external solutions, and transport currents were calculated by subtracting amplitudes before glutamate application from amplitudes obtained in the presence of glutamate. Current amplitudes were measured at the end of voltage steps that were long enough to reach steady-state conditions (glutamate uptake: 50 ms, Figure 3; anion current with K^+_{int}: 100 ms, Figures 4, S1, and S3–S5; anion current with Na^+_{int}: 150 ms, Figures 5 and S4). Cell capacitances (C_{slow}) were estimated using built-in capacitance compensation of the EPC-10 amplifier or manual capacitance compensation of the Axon 200 A amplifier. In all experiments, we used external and internal agar salt bridges made from plastic tubes filled with 3 M KCl in 1.0% agar to connect the Ag/AgCl electrodes. Junction potentials were calculated with Clampex 10.5 and corrected. Background currents were determined in untransfected HEK293T cells or in HEK293T cells transfected with WT *h*EAAT1 after 5′ incubation with the specific EAAT1 inhibitor UCPH-101 (10 µM, 2-Amino-4-(4-methoxyphenyl)−7-(naphthalen-1-yl)−5-oxo-5,6,7,8-tetrahydro-4H-chromene-3-carbonitrile; Abrahamsen et al., 2013).

2.4 | Statistics

Data are presented as means ($\bar{x}$) ± 95% confidence interval (CI). Normality of data was tested with Shapiro–Wilk tests and variance homogeneity with the Levene test. Data were then analyzed either

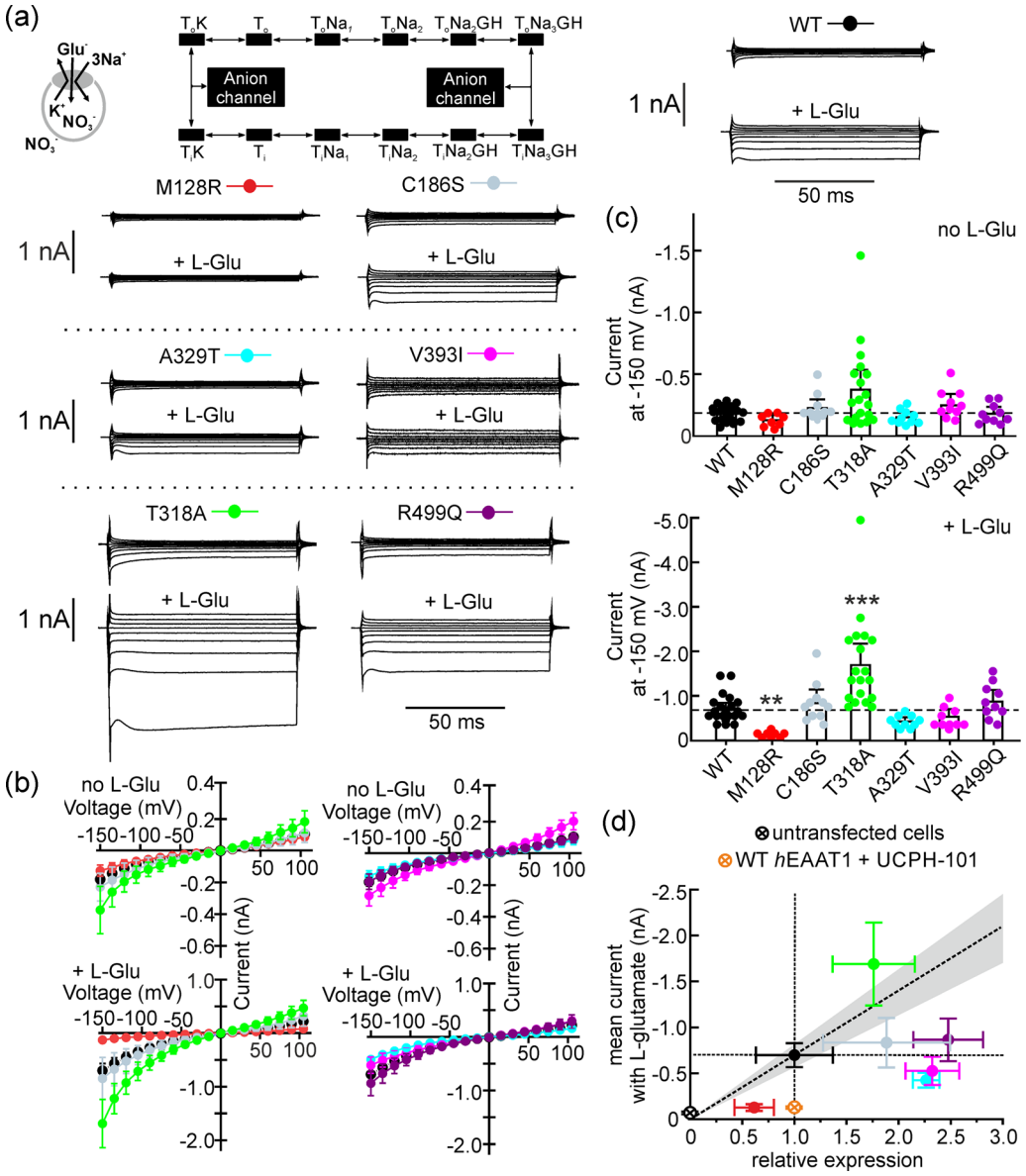

FIGURE 4 Anion currents of WT and mutant *h*EAAT1 variants under ionic conditions permitting glutamate uptake. (a) Representative whole-cell current recordings from HEK293T cells heterologously expressing WT or EA6-associated missense variants of *h*EAAT1. Currents before and after application of 0.5 mM L-glutamate in the bath solution are shown. The inset provides the ionic conditions during the experiment and the conformational states, which can be assumed by the transporter. (b) Current-voltage relationships of glutamate anion currents from WT and mutant *h*EAAT1 forms. Current amplitudes were measured 100 ms after the voltage jump. (c) Bar plots summarizing current amplitudes at −150 mV in the absence (top) and the presence (bottom) of 0.5 mM L-glutamate. (d) Plots of measured current amplitudes at −150 mV and expression levels of tested *h*EAAT1 variants. The dashed line connects the origin of the plot with mean current amplitudes/relative expression levels of WT *h*EAAT1 and permits prediction of normal current amplitudes at different expression levels. Untransfected cells (crossed circles) exhibited negligible whole-cell currents at −150 mV in the presence of L-glutamate (mean ± CI: −56.6 ± 18.7 pA, $n = 10$). Data were analyzed with Kruskal–Wallis analysis of variance on ranks and Holm-Sidak post hoc tests. Data points in (b) and (d), and bars in (c) are provided as mean values ± 95% CI. Dots in (c) represent values obtained from individual cells. WT, wild type

using one-way analysis of variance (ANOVA) tests, or Kruskal–Wallis ANOVA tests on ranks with Holm-Sidak or Dunn's post hoc testing. All statistical parameters and linear regressions were calculated with SigmaPlot version 12.4 (Systat Software) or OriginPro 2018 G (OriginLab). *A* values of $p \le .05$ were considered significant (*$p \le .05$, **$p \le .01$, and ***$p \le .001$). Significances from Dunn's post hoc testing are indicated as #.

3 | RESULTS

3.1 | Biogenesis and intracellular transport of mutant *h*EAAT1 mutants

Disease-causing mutations often change expression levels or the subcellular distribution of affected proteins (Jeng et al., 2020;

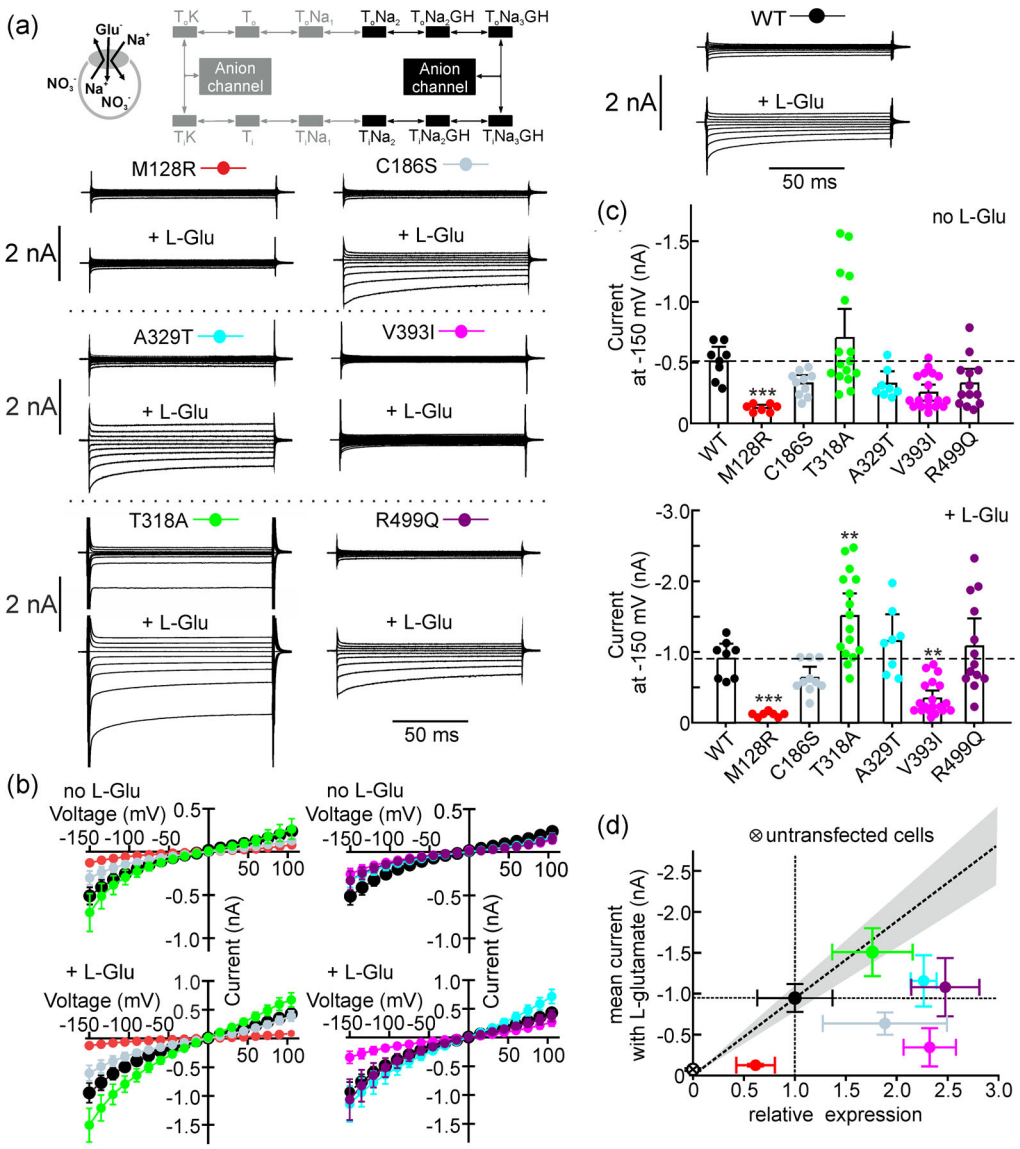

FIGURE 5 Anion currents of WT and mutant *h*EAAT1 variants under ionic conditions permitting Na^+ exchange. (a) Representative whole-cell current recordings from HEK293T cells heterologously expressing WT or EA6-associated missense variants of *h*EAAT1 before and after application of 0.5 mM L-glutamate to the bath solution. The inset shows the ionic conditions during the experiment and the conformational states, which can be assumed by the transporter. (b) Current voltage relationships of glutamate anion currents from WT and mutant *h*EAAT1 variants. Current amplitudes were measured 150 ms after the voltage jump. (c) Bar plots summarizing current amplitudes at −150 mV in the absence (top) and the presence (bottom) of 0.5 mM L-glutamate. (d) Plot of anion currents at −150 mV vs relative expression levels obtained in biochemical experiments. The dashed lines connect the origin of the plot with mean current amplitudes/relative expression levels of WT *h*EAAT1 and permit prediction of normal current amplitudes at different expression levels. Untransfected cells (crossed circles) exhibited negligible whole-cell currents at −150 mV in the presence of L-glutamate (−57 ± 21.7 pA, $n = 10$). Data were analyzed with Kruskal–Wallis analysis of variance on ranks and Holm-Sidak post hoc tests. Data points in (b) and (d), and bars in (c) are provided as mean values ± 95% CI. Dots in (c) represent values obtained from individual cells. EAAT1, excitatory amino acid transporter 1; WT, wild type

Ronstedt et al., 2015). To study whether EA6-associated mutations exert such effects, we expressed WT and mutant *h*EAAT1–YFP fusion proteins in HEK293T cells (Figure 2) and studied them with confocal microscopy and biochemical techniques. We observed similar substrate, time, and voltage dependences of *h*EAAT1 and *h*EAAT1–YFP anion current (Figure S1) indicating that transport functions are not modified by linking the YFP moiety to *h*EAAT1. We, therefore, performed all functional tests with YFP fusion proteins that will be designated as *h*EAAT1 in the following.

For all tested mutant transporters confocal images showed almost exclusive insertion into the surface membrane or in domains in close proximity (Figure 2a). We next resolved lysates from transfected HEK293T cells by SDS gel electrophoresis (Figure 2b), and estimated the transfection efficiencies of human EAAT1 variants

(Figure 2c). The transfection efficiencies were not significantly different from WT *h*EAAT1 so that protein amounts in cell lysates permit quantification of transcribed mutant proteins. Analysis of SDS-PAGE revealed unaltered mutant protein amounts for p.M128R and p.C186S (mean ratios to WT *h*EAAT1 ± CI: 0.71 ± 0.22/1.41 ± 0.56, $n = 9/7$, $p > .05^{n.s.}/>.05^{n.s.}$). The variants p.A329T, p.V393I, and p.R499Q increased total protein amount by a factor of 2 (2.0 ± 0.0.16/2.26 ± 0.33/2.17 ± 0.44, $n = 9/7/7$, $p < .001^{***}/<.001^{***}/<.001^{***}$), and p.T318A by a factor of 1.6 (1.65 ± 0.18, $n = 9$, $p < .01^{**}$; Figure 2d).

*h*EAAT1 can exist in non-, core-, or complex-glycosylated forms (Gendreau et al., 2004; Winter et al., 2012). The percentage of complex glycosylated protein represents a simple test for successful transporter exit from the ER. For WT as well as for all mutant *h*EAAT1 core- or complex-glycosylated states are predominant and result in the occurrence of two major fluorescent bands in SDS-PAGE (Figure 2b). We observed a slight reduction in the percentage of complex glycosylated protein for p.M128R (mean ± CI: 86 ± 9%, $n = 9$, $p < .05^{*}$) and a slight increase for p.C186S *h*EAAT1–YFP (114 ± 11%, $n = 7$, $p < .05^{*}$; Figure 2e).

3.2 | EA6-associated mutations exert multiple effects on *h*EAAT1 glutamate uptake

*h*EAAT1 transports glutamate stoichiometrically coupled to three Na^+ and one H^+ in exchange with one K^+ (Zerangue & Kavanaugh, 1996). Each uptake cycle is associated with the net transport of two positive charges, and glutamate transport can thus be quantified using electrophysiological techniques by subtracting current amplitudes measured before glutamate application from amplitudes obtained in the presence of the substrate. Since EAATs also function as anion channels, permeable anions have to be replaced with non-permeable anions to measure uptake currents in isolation (Wadiche, Amara & Kavanaugh, 1995). Figure 3a shows representative subtracted whole-cell currents of HEK293T cells expressing WT or mutant *h*EAAT1. Cells expressing WT *h*EAAT1 showed robust voltage-dependent uptake currents with a mean of −183 ± 39 pA (±CI, $n = 8$) at −150 mV. The mutation p.T318A increased uptake currents (mean ± CI: −296 ± 72 pA, $n = 11$, $p < .05^{*}$), whereas p.M128R resulted in an almost complete disappearance of transport (mean ± CI: −12 ± 14 pA, $n = 7$, $p < .001^{***}$). The mutations p.V393I (−109 ± 37 pA, ±CI, $n = 9$, $p > .05^{n.s.}$), p.C186S (−101 ± 61 pA, $n = 6$, $p > .05^{n.s.}$), p.R499Q (−190 ± 55 pA, ±CI, $n = 8$, $p > .05^{n.s.}$), and p.A329T (−199 ± 37 pA, $n = 8$, $p > .05^{n.s.}$) showed similar uptake currents as WT *h*EAAT1 (Figure 3b,c). To account for the different expression levels (Figure 2), we plotted current amplitudes versus mean expression levels of complex glycosylated transporter protein obtained by multiplying relative protein expression levels (Figure 2d) and the percentage of complex glycosylated proteins (Figure 2e). This plot compares mean uptake currents and mean expression levels for WT and mutant *h*EAAT1 (Figure 3d) and demonstrates that transport rates normalized to expression levels were reduced for all variants—with exception of p.T318A. The mutation p.T318A *h*EAAT1 showed glutamate uptake levels that were increased in parallel to its higher expression level in HEK293T cells (Figure 3d). Figure S2 depicts plots of glutamate uptake currents versus capacitances of cells expressing WT or mutant transporters and a comparison of glutamate transport current densities that were obtained from the slopes of these relationships. Individual mutants exert similar effects on uptake currents and uptake current densities, demonstrating that the expression levels rather than cell sizes determine the amplitudes of the whole-cell currents.

3.3 | Anion currents of WT and mutant *h*EAAT1

EAAT anion channels open upon lateral movement of the transport domain from intermediate translocation states (Machtens et al., 2015). The kinetics of EAAT anion currents are thus tightly linked to transitions within the glutamate uptake cycle (Fahlke et al., 2016; Otis & Kavanaugh, 2000), and changes in anion current kinetics provide insights into possible disease-associated alterations within the *h*EAAT1 uptake cycle. We studied *h*EAAT1 anion currents under two different ionic conditions. Whereas the transporter can move through the whole transport cycle in cells intracellularly dialyzed with a KNO_3-based solution (Figure 4a), the use of $NaNO_3$-based solutions restricts the accessible states to the so-called Na^+-hemicycle (Figure 5a).

Figure 4a shows representative whole-cell current responses to voltages between −150 mV and +90 mV from HEK293T cells expressing WT or mutant *h*EAAT1 internally dialyzed with a K^+-based solution. The use of the more permeant anion NO_3^- enhances *h*EAAT1 anion currents and permits recording such currents without significant contamination of background currents (at −150 mV, untransfected cells in the presence of L-glutamate: mean ± CI: −56.6 ± 18.7 pA, WT *h*EAAT1 + 10 μM UCPH-101: −127 ± 4.7 pA, $n = 10/3$, Figures 4 and S3; Kovermann et al., 2017; Kovermann, Machtens, Ewers, & Fahlke, 2010). Application of 0.5 mM L-glutamate resulted in a fourfold increase (mean ± CI: 4.2 ± 1.0) of the WT *h*EAAT1 current amplitude (mean ± CI: − 180 ± 26/−698 ± 130 pA, $n = 21$) at −150 mV (Figure S4a; Kovermann et al., 2017; Winter et al., 2012). The mutation p.M128R abolished anion currents in the presence of glutamate (mean ± CI: −128 ± 36 pA, $n = 8$, $p < .01^{**}$; Figures 4a–c and S4a). The p.T318A *h*EAAT1 anion currents were slightly larger than WT before (mean ± CI: 374 ± 150 pA) and much larger after glutamate application (−1689 ± 451 pA, $n = 19$, $p > .05^{n.s.}/<.001^{***}$; Figure 4a–c), with normal glutamate-induced increases ($p > .05^{n.s.}$; Figure S4a) and identical voltage dependence to WT *h*EAAT1 ($p > .05^{n.s.}$; Figure S5). The variants p.V393I (mean ± CI: −258 ± 68 pA/484 ± 136 pA), p.C186S (mean ± CI: −225 ± 62/−833 ± 270 pA), p.A329T (mean ± CI: −144 ± 34/−421 ± 81 pA), and p.R499Q (mean ± CI: −178 ± 49/−866 ± 232 pA) left anion currents with and without glutamate unaffected ($n = 10/11/10/10$, $p > .05^{n.s.}/>.05^{n.s.}/>.05^{n.s.}/>.05^{n.s.}$; Figure 4a–c). We did not observe pronounced alterations in the time or voltage dependence for any of the tested

mutants, in the absence as well as in the presence of glutamate. Normalization of anion currents by the relative protein expression shows that p.T318A increases macroscopic anion current amplitudes by boosting the expression levels, whereas all other variants decrease normalized anion currents in the presence or absence of external glutamate (Figure 4d). Again, the effects of individual mutations on mean anion currents and mean anion current densities were quite similar (Figure S6) supporting our notion that expression levels rather than cell sizes determine the amplitudes of the whole-cell currents.

We next tested anion currents of WT and mutant proteins with Na^+ as main intracellular cation, as indicated in the inset (Figure 5). The reduced number of accessible states within the transport cycle results in a change of current kinetics and a reduced increase upon glutamate application (mean ± CI: − 510 ± 100/−906 ± 176 pA, $n = 8$; Figure 5a). However, disease-associated mutations induce similar changes in function as observed with K^+ as main intracellular cation (Figure 5a–c and S4b). The variant p.M128R abolished anion currents without or with glutamate (mean ± CI: −127 ± 19/−124 ± 20 pA, $n = 7$, $p < .001^{***}/<.001^{***}$), and p.T318A increases anion currents only in the presence of glutamate (mean ± CI: −703 ± 220/−1508 ± 293 pA, $n = 16$, $p > .05^{n.s.}/<.01^{**}$; Figure 5c). When measured in cells dialyzed with Na^+-based solutions, p.V393I did not enhance anion currents in glutamate-free solutions (mean ± CI: −252 ± 62 pA, $p > .05^{n.s.}$), but prevented glutamate-induced changes in current amplitudes (mean ± CI: −344 ± 105 pA, $n = 19$, $p < .01^{**}$; Figures 5c and S4b). Also under these ionic conditions p.C186S (mean ± CI: −328 ± 57/−635 ± 137 pA), p.A329T (mean ± CI: −327 ± 83/−1157 ± 313 pA), and p.R499Q (mean ± CI: −328 ± 108/−1080 ± 356 pA) left anion currents with and without glutamate unaffected ($n = 10/8/13$, $p > .05^{n.s.}/>.05^{n.s.}/>.05^{n.s.}$; Figures 5a–c and S4b). However, the combined analysis of expression and current amplitudes revealed that p.T318A increases macroscopic anion current amplitudes by augmenting expression levels, whereas all other variants decrease normalized anion currents in the presence or absence of external glutamate (Figure 5d).

3.4 | Coexpression of WT and mutant *h*EAAT1

At present, *SLC1A3* mutations have only been reported in heterozygous patients. *h*EAAT1 assemble as trimers (Gendreau et al., 2004; Nothmann et al., 2011), and individual subunits independently function as glutamate transporter and anion channel (Grewer et al., 2005; Brown, Koch, & Larsson, 2007; Leary, Stone, Holley, & Kavanaugh, 2007). The lack of functional interaction between monomers let dominant negative functional effects of individual mutant subunits on neighboring WT subunit appear unlikely in heterozygous patients. However, impaired trafficking of individual subunits might result in retention of heteromeric transporters.

We performed coexpression experiments of WT and mutant transporters for the mutations with most pronounced functional alterations among the tested sequence variations. Figure 6 depicts representative recordings of cells coexpressing WT *h*EAAT1 and p.M128R *h*EAAT1 (Figure 6a) or WT *h*EAAT1 and p.T318A *h*EAAT1 (Figure 6c). Figures 6b and 6d show mean current–voltage relationships from cells expressing WT or mutants alone or coexpressing WT and mutant *h*EAAT1 variants under standard conditions with nitrate as permeable anion (in mM, ext: 140 $NaNO_3$, int: 110 KNO_3, pH 7.4). Coexpression of p.M128R *h*EAAT1 reduces glutamate-activated currents of WT *h*EAAT1 at −150 mV (mean ± CI: −698 ± 130 pA [WT *h*EAAT1], −400 ± 96 pA [WT *h*EAAT1::p.M128R *h*EAAT1], $n = 21/10$; Figures 6a,b and 6e). We tested the specificity of interaction by coexpressing WT *h*EAAT1 with p.E281Q ClC-4 (NM_0018430.4: c.841G>C), a mutant Cl^-/H^+ exchanger that exclusively generates capacitive transients (Alekov & Fahlke, 2009; Guzman et al., 2013). This maneuver did not reduce WT *h*EAAT1 anion currents (mean ± CI: −628 ± 143 pA [WT *h*EAAT1::p.E281Q *h*ClC-4]; Figures 6d and 6g), indicating that WT-p.M128R heterotrimers exhibit reduced surface insertion in agreement with reduced glycosylation rate in p.M128R *h*EAAT1 (Figure 2d). Coexpression of p.T318A augments WT currents at −150 mV (mean ± CI: −2,017 ± 683 pA, $n = 10$) to values as expected by nonfunctionally interacting subunits (Figures 6c,d and 6f).

4 | DISCUSSION

Episodic ataxia is characterized by attacks of incoordination, imbalance, and inter-attack weakness, often associated with progressive ataxia, epilepsy, dystonia, or hemiplegic migraine (Jen et al., 2007). The spectrum of neurological symptoms indicates a cerebellar origin, and indeed all known episodic ataxia disease genes encode cerebellar proteins. Approximately 2/3 of all cases with episodic ataxia carry mutations in *KCNA1* (EA1) or *CACNA1A* (EA2) (Jen et al., 2007). Mutations in *CACNB4* (Escayg et al., 2000) were associated with EA5 and in *SLC1A3* with EA6. Since all proteins encoded by EA disease genes likely contribute to synaptic transmission in the cerebellum, EA6-associated *SLC1A3* mutations were initially assumed to modify glutamatergic synaptic transmission via reduced glutamate reuptake capability.

Our group studied the functional consequences of the p.P290R mutation in *SLC1A3*, which was reported for the first and most severe case of EA6 (Jen et al., 2005), using heterologous expression and cellular electrophysiology (Hotzy et al., 2013; Winter et al., 2012). We found that p.P290R decreases glutamate transport rates, but increased absolute open probabilities of EAAT1 anion channels. We proposed that gain-of-function of p.P290R *h*EAAT1 anion channels decreases anion concentrations in Bergmann glia (Untiet et al., 2017) and hypothesized that the resulting increase in driving force of GATs (GABA transporters) might reduce import of GABA and thus inhibitory synaptic transmission in the EA6 patient (Winter et al., 2012). However, a transgenic animal that is heterozygous for the p.P290R mutation ($Slc1a^{P290R/+}$) demonstrated a rather distinct disease mechanism. The p.P290R knock-in animals exhibited Bergmann glia degeneration between P10 and P20, presumably because

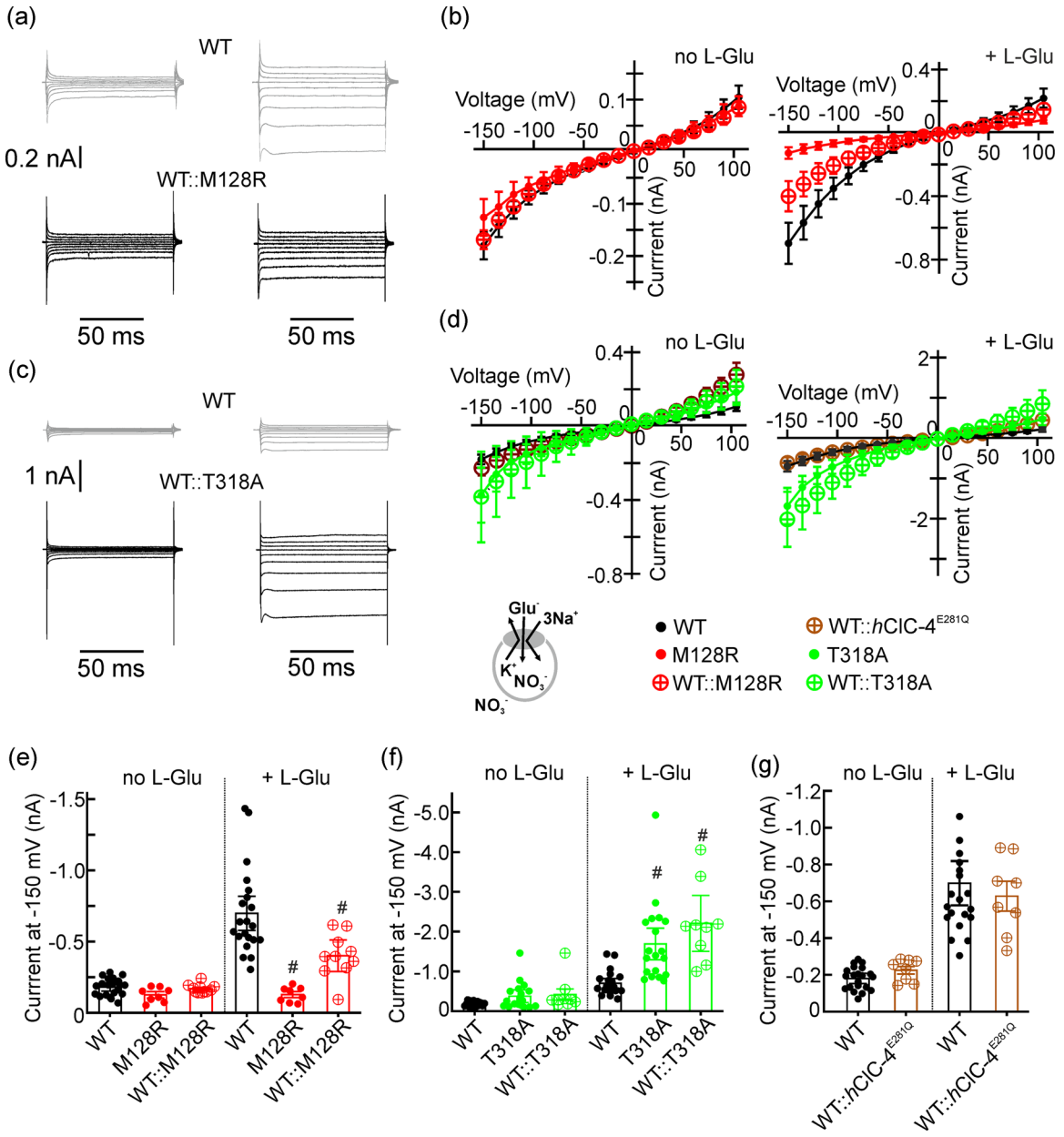

FIGURE 6 Coexpression of WT and EA6-associated mutant *h*EAAT1. (a and c) Representative current traces from cells expressing WT *h*EAAT1 alone (a and c, gray) or coexpressing WT and p.M128R *h*EAAT1 (black, a) or WT and p.T318A *h*EAAT1 (black, c). (b and d) Current–voltage relationships from cells expressing p.M128R (b, red crossed circles) and WT *h*EAAT1 (b, black circles) or p.T318A *h*EAAT1 (b, green circles) and from cells coexpressing WT and T318A *h*EAAT1 (b, green-crossed circles) or WT (b, black circles) and M128R *h*EAAT1 (b, green circles) under standard ionic conditions (in mM, ext: 140 $NaNO_3$ ± 0.5 L-Glu, int: 110 KNO_3, pH 7.4). (e–g) Bar plots summarize current amplitudes at −150 mV for WT *h*EAAT1 (e–g, black circles), p.M128R *h*EAAT1 (e, red circles), coexpression of WT and p.M128R (e, red crossed circles), T318A *h*EAAT1 (f, green circles), coexpression of WT and p.T318A (f, green crossed circles), and coexpression of WT *h*EAAT1 with p.E281Q *h*ClC-4 (g, brown crossed circles). Data points in (b), (d), and bars in (e)–(g) are provided as mean values ± 95% CI. Dots in (e)–(g) represent values obtained from individual cells. EAAT1, excitatory amino acid transporter 1, WT, wild type

of enhanced Cl^- efflux, cell shrinkage, and subsequent apoptosis (Kovermann et al., 2020). The lack of Bergmann glia results impairs glutamate re-uptake, modifies synaptic transmission in the cerebellum, and causes generalized cerebellar degeneration in a certain percentage of transgenic animals. Thus, p.P290R causes a dramatic reduction in cerebellar glutamate uptake, albeit primarily affecting EAAT1 anion channel activity.

We here studied the functional consequences of the remaining six published EA6 mutations using similar approaches we originally applied to p.P290R (Winter et al., 2012). We compared the effects of EA6 mutations on EAAT1 expression, glycosylation, subcellular distribution (Figure 2), glutamate uptake currents (Figure 3) as well as on anion currents under two ionic conditions, that is, with K^+ (Figure 4) or with Na^+ (Figure 5) as main intracellular cation. For all

tested mutations, the subcellular distribution as well as the fluorescence of transfected cells were similar to WT. We tested the percentage of complex glycosylated proteins, and observed slightly reduced complex glycosylation levels in p.M128R, slightly increased ones in p.C186S, and unaltered glycosylation of the remaining mutants. Expression levels of p.T318A, p.A329T, p.V393I, and p.R499Q *h*EAAT1 were approximately twofold increased. Although subcellular trafficking was not dramatically reduced and expression levels were only slightly reduced for p.M128R EAAT1, we could neither observe glutamate uptake nor anion currents, indicating loss-of-function of this mutant. However, p.M128R *h*EAAT1 reduce WT *h*EAAT1 currents in coexpression experiments (Figure 6), suggesting that trafficking of heterotrimers consisting of WT and p.M128R subunits is impaired.

We observed the highest amplitudes for glutamate uptake current and anion currents for p.T318A *h*EAAT1. The p.T318A *h*EAAT1 current amplitudes were increased as expected by the enhanced expression of this mutant (Figures 3d, 4d, 5d). Moreover, time, voltage, and substrate dependence of p.T318A *h*EAAT1 anion currents were indistinguishable from WT (Figure 4 and 5; Figure S5). This analysis indicates that p.T318A neither affects trafficking nor function, but exclusively *h*EAAT1 expression. The variant p.V393I *h*EAAT1 exhibited normal glutamate transport currents and normal anion currents with K^+ as main cation in the absence of glutamate. (Figure 4). In cells dialyzed internal Na^+, the p.V393I *h*EAAT1 anion current amplitudes were very small in the absence of glutamate and virtually did not increase upon glutamate application (Figure 5). These changes in substrate sensitivity, together with the decreased normalized uptake currents (Figure 3d) indicate that p.V393I impairs glutamate transport activity via modification of the transport cycle.

For p.C186S, p.A329T, and p.R499Q, neither changes in uptake nor anion current amplitudes were observed. Substrate and voltage dependence of anion currents were closely similar to WT, arguing against profound changes in the uptake cycle. Since expression levels were significantly increased for p.A329T and p.R499Q, and complex glycosylation enhanced for C186S, we conclude that p.C186S, p.A329T, and p.R499Q impair late steps in membrane surface insertion of *h*EAAT1 and thus reduce macroscopic glutamate uptake and anion currents. This conclusion does not contradict the unaltered subcellular distribution of *h*EAAT1 fluorescent fusion proteins (Figure 2a) since the restricted optical resolution of confocal images prevents distinction between surface membrane insertion and localization in close proximity to the membrane.

Some of the observed functional alterations in heterologous expression systems permit predictions about changes in glial membrane transport in affected patients, while others are more difficult to interpret. The mutation p.M128R abolishes *h*EAAT1 glutamate transport and anion current to loss-of-function levels. Patients carrying the p.M128R mutations are thus expected to exhibit a 50% reduction in EAAT1 glutamate transport and anion current. The variant p.T318A increases glutamate uptake and anion currents approximately twofold. We cannot conclude with certainty that *h*EAAT1 expression will be similarly increased in patients. However, such change in transporter biogenesis would correspond to anion current enhancements in Bergmann glia of heterozygous patients, which is roughly equivalent to the changes we observed in the knock-in animal model *Slc1a3*$^{P290R/+}$ (Kovermann et al., 2020). The glutamate independent of p.V393I *h*EAAT1 anion currents in cells dialyzed with Na^+-based solutions (Figure 5) suggests that Na^+-bound translocation is severely impaired, and such an alteration would also explain the reduced normalized glutamate transport (Figure 3d). Moreover, normalized glutamate transport by p.V393I *h*EAAT1 (Figure 3d) is lower than that for WT *h*EAAT1 and might contribute to reduced glutamate uptake in patients carrying the corresponding *SLC1A3* mutation.

The consequences of p.C186S, p.A329T, and p.R499Q in patients carrying the causal *SLC1A3* mutations are difficult to predict. The p.C186S mutations was already evaluated using radiotracer flux measurements in COS7 cells transfected with WT or mutant EAAT1 and found to decrease individual uptake rates by 18% (de Vries et al., 2009). In our experiments, we observed a slightly increased complex glycosylation (Figure 2) and a decreased normalized glutamate uptake capability (Figure 3). The remaining mutations, that is, p.A329T and p.R499Q, increase the expression levels, but leave transport and anion currents unaltered. A similar alteration in native cells would leave *h*EAAT1 function unaltered in patients. However, if expression levels are controlled to identical levels in normal individuals and in patients, our results would predict moderately reduced glutamate uptake in episodic ataxia patients with these *SLC1A3* mutations.

Thus far, we have only tested the consequences of p.M128R, p.C186S, p.T318A, p.A329T, p.V393I, and p.R499Q in heterologous expression systems. Since electrophysiological changes in *Slc1a3*$^{P290R/+}$ Bergmann glia anion currents are in good agreement with prediction from p.P290R *h*EAAT1 function in transfected HEK293T cells (Kovermann et al., 2020; Winter et al., 2012), we are confident that changes in transport functions, such as those observed in p.M128R and in p.V393I, can be translated to altered mutant *h*EAAT1 function in native tissue. Expression and subcellular trafficking in Bergmann glia cells from patients likely differs from transfected HEK293T cells, so that the pronounced effects of p.T318A or the small alterations of p.C186S, p.A329T, p.V393I, and p.R499Q should be further tested in transgenic animal experiments.

The patient carrying the p.P290R mutation has far most severe symptoms among the reported EA6 cases, with severe episodic and progressive ataxia, seizures, alternating hemiplegia, and migraine. We now tested multiple disease-associated mutations, and it was therefore tempting to compare the mutants' consequences on transporter function after heterologous expression and the severity of symptoms. The mutations analyzed in this study caused less pronounced changes in transport functions than those observed for p.P290R (Winter et al., 2012), and symptoms were milder than that for the p.P290R patient (Jen et al., 2005). However, among the remaining EA6 mutations we did not observe a clear correlation of the functional impairments of *h*EAAT1 in our experiments and the reported clinical symptoms. The p.M128R mutation had the most pronounced effects

on *h*EAAT1 function, that is, loss-of-function of homotrimetric transporters and dominant negative effects in coexpression studies. The p.M128R variant was described in a patient who suffered from episodes of truncal ataxia, strabismus, intentional tremor, and slurred speech (Iwama et al., 2017). Another mutation, p.T318A, had opposite effects on *h*EAAT1 functions. It enhanced *h*EAAT1 expression resulting in larger glutamate uptake and anion currents, but caused more severe symptoms, that is, ataxia, dizziness, dysarthria, gaze-evoked nystagmus, rebound upbeat nystagmus, and cognitive impairment (Choi, Kim, et al., 2017). Both, p.C186S and p.V393I caused only mild reductions in *h*EAAT1glutamate uptake and anion currents. Patients with these mutations exhibited similar clinical symptoms (Choi, Jen, et al., 2017; de Vries et al., 2009), however, the disease onset was very late (in the sixth decade of life) for patients with p.V393I. The variants p.A329T and p.R499Q had the least severe effects on *h*EAAT1 function, and the p.A329T mutation was found in a patient with an additional *CACNA1A* mutation (Choi, Kim, et al., 2017), which might also contribute to the disease phenotype. For p.A329T ataxia, dizziness, and gaze-evoked nystagmus seizure were reported, whereas p.R499Q was only associated with speech disturbance and upper limb clumsiness.

SLC1A3 mutations have not only been found in patients with episodic ataxia 6, but also in migraine (Kovermann et al., 2017); Tourette syndrome (Adamczyk et al., 2011); attention deficit hyperactivity disorder (ADHD), and autism (van Amen-Hellebrekers et al., 2016). In a recent case with familial migraine, the patient was heterozygous for the missense mutation p.T387P (NM_004172.4: c.1159A>C), which renders EAAT1 completely transport incompetent (Kovermann et al., 2017) by preventing K^+ bound retranslocation (Kortzak et al., 2019). This functional consequence resembles our results on M128R. Patients carrying the p.M128R mutations also expressed only functional WT transporter together with a nonfunctional mutant. However, the neurological symptoms of the patients were quite distinct. During migraine attacks the patient carrying the p.T387P mutation experienced visual disturbances, prominent dysphasia, and hemiparesis (Kovermann et al., 2017). The patient with the p.M128R suffered from early onset ataxia, with truncal ataxia and strabismus. In heterologous expression systems the sequence variant predicting p.E219D *h*EAAT1 (NM_004172.4: c.657G>C), which was associated with Tourette syndrome (Adamczyk et al., 2011), stimulated surface membrane insertion of the transporter. At present, it is not clear whether similar changes in trafficking will also occur in patients' glia cells. Moreover, *SLC1A3* duplications might increase glutamate uptake and anion currents of glia cells in ADHD and autism (van Amen-Hellebrekers et al., 2016). However, the neurological symptoms are quite different for patients carrying these distinct genetic changes. One might speculate that increased glutamate transport and anion channel activity might alter neuronal migration and thus neuronal network formation and function. The different *SLC1A3* mutations that enhance translation (*SLC1A3* duplication), transcription (p.T318A), or surface membrane insertion (p.E219D) might affect EAAT1 transporter function in different developmental stages and thus cause distinct neurological changes.

Episodic ataxia 6 is a rare disease, and only few EA6-associated *SLC1A3* mutations have been reported, with small numbers of affected patients per family. In several cases, the family members who carry the same *SLC1A3* mutations that was found in the EA6 patients do not suffer from episodic ataxia. We tested six missense mutations that were reported in patients with episodic ataxia in heterologous expressions systems. We found distinct alterations of *h*EAAT1 function and/or expression for each of the *SLC1A3* mutations and demonstrated that episodic ataxia 6 can be associated with impaired as well as with enhanced *h*EAAT1 glutamate transport and/or anion current. The variants p.M128R and p.V393I caused changes in *h*EAAT1 transport and/or anion channel activity. The p.T381A mutation enhanced both *h*EAAT1 uptake and anion currents. For the remaining three, normal current amplitudes at increased expression levels suggested impaired glutamate uptake and anion currents. Taken together, genetic and functional data illustrated the importance of modifying genetic or environmental factors in determining the disease phenotype of *SLC1A3*-associated diseases. Our findings suggested that even small alterations can result in clinically significant alteration in cerebellar function, demonstrating how sensibly the cerebellum reacts on even slight alterations of *h*EAAT1 function.

ACKNOWLEDGMENTS

We are grateful to Yulia Kolobkova and Miriam Engels for helpful discussions, and also Arne Franzen and Petra Thelen for their excellent technical assistance. This study was supported by the German Ministry of Education and Research (E-RARE network Treat-ION, BMBF 01GM1907C to C. F.). Open access funding enabled and organized by Projekt DEAL.

CONFLICTS OF INTEREST

The authors declare no conflict of interest.

DATA AVAILABILITY STATEMENT

The data that support the findings of this study are openly available in GitHub at https://github.com/dkortzak/episodic_ataxia_6.

ORCID

Aparna S. Chivukula http://orcid.org/0000-0002-5191-9872
Daniel Kortzak https://orcid.org/0000-0001-9098-3466
Peter Kovermann http://orcid.org/0000-0001-5296-4918
Christoph Fahlke https://orcid.org/0000-0001-8602-9952

REFERENCES

Abrahamsen, B., Schneider, N., Erichsen, M. N., Huynh, T. H., Fahlke, C., Bunch, L., & Jensen, A. A. (2013). Allosteric modulation of an excitatory amino acid transporter: The subtype-selective inhibitor UCPH-101 exerts sustained inhibition of EAAT1 through an intramonomeric site in the trimerization domain. *Journal of Neuroscience*, *33*, 1068–1087. https://doi.org/10.1523/JNEUROSCI.3396-12.2013

Adamczyk, A., Gause, C. D., Sattler, R., Vidensky, S., Rothstein, J. D., Singer, H., & Wang, T. (2011). Genetic and functional studies of a missense variant in a glutamate transporter, SLC1A3, in Tourette syndrome. *Psychiatric Genetics*, *21*, 90–97. https://doi.org/10.1097/YPG.0b013e328341a307

Alekov, A., & Fahlke, C. (2009). Channel-like slippage modes in the human anion/proton exchanger ClC-4. *Journal of General Physiology*, *133*, 485–496. https://doi.org/10.1085/jgp.200810155

van Amen-Hellebrekers, C. J., Jansen, S., Pfundt, R., Schuurs-Hoeijmakers, J. H., Koolen, D. A., Marcelis, C. L., & de Vries, B. B. (2016). Duplications of *SLC1A3*: Associated with ADHD and autism. *European Journal of Medical Genetics*, *59*, 273–376. https://doi.org/10.1016/j.ejmg.2016.06.003

Cader, M. Z., Steckley, J. L., Dyment, D. A., McLachlan, R. S., & Ebers, G. C. (2005). A genome-wide screen and linkage mapping for a large pedigree with episodic ataxia. *Neurology*, *65*, 156–158. https://doi.org/10.1212/01.wnl.0000167186.05465.7c

Canul-Tec, J. C., Assal, R., Cirri, E., Legrand, P., Brier, S., Chamot-Rooke, J., & Reyes, N. (2017). Structure and allosteric inhibition of excitatory amino acid transporter 1. *Nature*, *544*, 446–451. https://doi.org/10.1038/nature22064

Choi, K. D., Jen, J. C., Choi, S. Y., Shin, J. H., Kim, H. S., Kim, H. J., & Choi, J. H. (2017). Late-onset episodic ataxia associated with *SLC1A3* mutation. *Journal of Human Genetics*, *62*, 443–446. https://doi.org/10.1038/jhg.2016.137

Choi, K. D., Kim, J. S., Kim, H. J., Jung, I., Jeong, S. H., Lee, S. H., & Choi, J. H. (2017). Genetic variants associated with episodic ataxia in Korea. *Scientific Reports*, *7*, 13855. https://doi.org/10.1038/s41598-017-14254-7

Chivukula, A. S., Suslova, M., Kortzak, D., Kovermann, P., & Fahlke, C. (2000). Functional consequences of SLC1A3 mutations associated with episodic ataxia 6, GitHub [Data set]. Retrieved from https://github.com/dkortzak/episodic_ataxia_6

Conroy, J., McGettigan, P., Murphy, R., Webb, D., Murphy, S. M., McCoy, B., & Ennis, S. (2014). A novel locus for episodic ataxia: *UBR4* the likely candidate. *European Journal of Human Genetics*, *22*, 505–510. https://doi.org/10.1038/ejhg.2013.173

Corbett, M. A., Bellows, S. T., Li, M., Carroll, R., Micallef, S., Carvill, G. L., & Gecz, J. (2016). Dominant *KCNA2* mutation causes episodic ataxia and pharmacoresponsive epilepsy. *Neurology*, *87*(19), 1975–1984. https://doi.org/10.1212/WNL.0000000000003309

Damji, K. F., Allingham, R. R., Pollock, S. C., Small, K., Lewis, K. E., Stajich, J. M., & Pericak-Vance, M. A. (1996). Periodic vestibulocerebellar ataxia, an autosomal dominant ataxia with defective smooth pursuit, is genetically distinct from other autosomal dominant ataxias. *Archives of Neurology*, *53*, 338–344. https://doi.org/10.1001/archneur.1996.00550040074016

Escayg, A., De Waard, M., Lee, D. D., Bichet, D., Wolf, P., Mayer, T., & Meisler, M. H. (2000). Coding and noncoding variation of the human calcium-channel beta4-subunit gene *CACNB4* in patients with idiopathic generalized epilepsy and episodic ataxia. *American Journal of Human Genetics*, *66*, 1531–1539. https://doi.org/10.1086/302909

Fahlke, C., Kortzak, D., & Machtens, J. P. (2016). Molecular physiology of EAAT anion channels. *Pflügers Archiv-European Journal of Physiology*, *468*, 491–502. https://doi.org/10.1007/s00424-015-1768-3

Garcia-Olivares, J., Alekov, A., Boroumand, M. R., Begemann, B., Hidalgo, P., & Fahlke, C. (2008). Gating of human ClC-2 chloride channels and regulation by carboxy-terminal domains. *Journal of Physiology*, *586*, 5325–5336. https://doi.org/10.1113/jphysiol.2008.158097

Gendreau, S., Voswinkel, S., Torres-Salazar, D., Lang, N., Heidtmann, H., Detro-Dassen, S., & Fahlke, C. (2004). A trimeric quaternary structure is conserved in bacterial and human glutamate transporters. *Journal of Biological Chemistry*, *279*, 39505–39512. https://doi.org/10.1074/jbc.M408038200

Grewer, C., Balani, P., Weidenfeller, C., Bartusel, T., Tao, Z., & Rauen, T. (2005). Individual subunits of the glutamate transporter EAAC1 homotrimer function independently of each other. *Biochemistry*, *44*, 11913–11923. https://doi.org/10.1021/bi050987n

Guzman, R., Grieschat, M., Fahlke, C., & Alekov, A. (2013). ClC-3 is an intracellular chloride/proton exchanger with large voltage-dependent nonlinear capacitance. *American Chemical Society: Chemical Neuroscience*, *4*, 994–1003. https://doi.org/10.1021/cn400032z

Hotzy, J., Schneider, N., Kovermann, P., & Fahlke, C. (2013). Mutating a conserved proline residue within the trimerization domain modifies Na^+ binding to excitatory amino acid transporters and associated conformational changes. *Journal of Biological Chemistry*, *288*, 36492–36501. https://doi.org/10.1074/jbc.M113.489385

Iwama, K., Iwata, A., Shiina, M., Mitsuhashi, S., Miyatake, S., Takata, A., & Matsumoto, N. (2017). A novel mutation in *SLC1A3* causes episodic ataxia. *Journal of Human Genetics*, *63*, 207–211. https://doi.org/10.1038/s10038-017-0365-z

Jen, J. C., Graves, T. D., Hess, E. J., Hanna, M. G., Griggs, R. C., & Baloh, R. W. (2007). Primary episodic ataxias: Diagnosis, pathogenesis and treatment. *Brain*, *130*, 2484–2493. https://doi.org/10.1093/brain/awm126

Jen, J. C., Wan, J., Palos, T. P., Howard, B. D., & Baloh, R. W. (2005). Mutation in the glutamate transporter EAAT1 causes episodic ataxia, hemiplegia, and seizures. *Neurology*, *65*, 529–534. https://doi.org/10.1212/01.wnl.0000172638.58172.5a

Jeng, C. J., Fu, S. J., You, C. Y., Peng, Y. J., Hsiao, C. T., Chen, T. Y., & Tang, C. Y. (2020). Defective gating and proteostasis of human ClC-1 chloride channel: Molecular pathophysiology of myotonia congenita. *Frontiers in Neurology*, *11*, 11. https://doi.org/10.3389/fneur.2020.00076

Kerber, K. A., Jen, J. C., Lee, H., Nelson, S. F., & Baloh, R. W. (2007). A new episodic ataxia syndrome with linkage to chromosome 19q13. *Archives of Neurology*, *64*, 749–752. https://doi.org/10.1001/archneur.64.5.749

Koch, H. P., Brown, R. L., & Larsson, H. P. (2007). The glutamate-activated anion conductance in excitatory amino acid transporters is gated independently by the individual subunits. *Journal of Neuroscience*, *27*, 2943–2947. https://doi.org/10.1523/JNEUROSCI.0118-07.2007

Kortzak, D., Alleva, C., Weyand, I., Ewers, D., Zimmermann, M. I., Franzen, A., & Fahlke, C. (2019). Allosteric gate modulation confers K^+ coupling in glutamate transporters. *EMBO Journal*, *38*, e101468. https://doi.org/10.15252/embj.2019101468

Kovermann, P., Hessel, M., Kortzak, D., Jen, J. C., Koch, J., Fahlke, C., & Freilinger, T. (2017). Impaired K^+ binding to glial glutamate transporter EAAT1 in migraine. *Scientific Reports*, *7*, 13913–13922. https://doi.org/10.1038/s41598-017-14176-4

Kovermann, P., Machtens, J. P., Ewers, D., & Fahlke, C. (2010). A conserved aspartate determines pore properties of anion channels associated with excitatory amino acid transporter 4 (EAAT4). *Journal of Biological Chemistry*, *285*, 23676–23686. https://doi.org/10.1074/jbc.M110.126557

Kovermann, P., Untiet, V., Kolobkova, Y., Engels, M., Baader, S., Schilling, K., & Fahlke, C. (2020). Increased glutamate transporter-associated anion currents cause glial apoptosis in episodic ataxia 6. *Brain Communications*, 2, fcaa022. https://doi.org/10.1093/braincomms/fcaa022

Leary, G. P., Stone, E. F., Holley, D. C., & Kavanaugh, M. P. (2007). The glutamate and chloride permeation pathways are colocalized in individual neuronal glutamate transporter subunits. *Journal of Neuroscience*, *27*, 2938–2942. https://doi.org/10.1523/JNEUROSCI.4851-06.2007

Machtens, J. P., Kortzak, D., Lansche, C., Leinenweber, A., Kilian, P., Begemann, B., & Fahlke, C. (2015). Mechanisms of anion conduction by coupled glutamate transporters. *Cell*, *160*, 542–553. https://doi.org/10.1016/j.cell.2014.12.035

Maksemous, N., Smith, R. A., Sutherland, H. G., Sampaio, H., & Griffiths, L. R. (2018). Whole-exome sequencing implicates *SCN2A* in Episodic Ataxia, but multiple ion channel variants may contribute to phenotypic complexity. *International Journal of Molecular Sciences*, *19*, 19. https://doi.org/10.3390/ijms19103113

Nothmann, D., Leinenweber, A., Torres-Salazar, D., Kovermann, P., Hotzy, J., Gameiro, A., … Fahlke, C. (2011). Hetero-oligomerization of neuronal glutamate transporters. *Journal of Biological Chemistry*, *286*, 3935–3943. https://doi.org/10.1074/jbc.M110.187492

Ophoff, R. A., Terwindt, G. M., Vergouwe, M. N., van Eijk, R., Oefner, P. J., Hoffman, S. M. G., & Frants, R. R. (1996). Familial hemiplegic migraine and episodic ataxia type-2 are caused by mutations in the Ca^{2+} channel gene *CACNL1A4*. *Cell*, *87*, 543–552. https://doi.org/10.1016/s0092-8674(00)81373-2

Otis, T. S., & Kavanaugh, M. P. (2000). Isolation of current components and partial reaction cycles in the glial glutamate transporter EAAT2. *Journal of Neuroscience*, *20*, 2749–2757. https://doi.org/10.1523/JNEUROSCI.20-08-02749.2000

Piarroux, J., Riant, F., Humbertclaude, V., Remerand, G., Hadjadj, J., Rejou, F., & Roubertie, A. (2020). *FGF14*-related episodic ataxia: Delineating the phenotype of Episodic Ataxia type 9. *Annals of Clinical and Translational Neurology*, *7*, 565–572. https://doi.org/10.1002/acn3.51005

Pyle, A., Smertenko, T., Bargiela, D., Griffin, H., Duff, J., Appleton, M., & Chinnery, P. F. (2015). Exome sequencing in undiagnosed inherited and sporadic ataxias. *Brain*, *138*, 276–283. https://doi.org/10.1093/brain/awu348

Reyes, N., Ginter, C., & Boudker, O. (2009). Transport mechanism of a bacterial homologue of glutamate transporters. *Nature*, *462*, 880–885. https://doi.org/10.1038/nature08616

Ronstedt, K., Sternberg, D., Detro-Dassen, S., Gramkow, T., Begemann, B., Becher, T., & Fahlke, C. (2015). Impaired surface membrane insertion of homo- and heterodimeric human muscle chloride channels carrying amino-terminal myotonia-causing mutations. *Scientific Reports*, *5*, 15382. https://doi.org/10.1038/srep15382

Schwarz, N., Bast, T., Gaily, E., Golla, G., Gorman, K. M., Griffiths, L. R., & Fazeli, W. (2019). Clinical and genetic spectrum of *SCN2A*-associated episodic ataxia. *European Journal of Paediatric Neurology*, *23*(3), 438–447. https://doi.org/10.1016/j.ejpn.2019.03.001

Schwarz, N., Hahn, A., Bast, T., Muller, S., Loffler, H., Maljevic, S., & Hedrich, U. B. S. (2016). Mutations in the sodium channel gene *SCN2A* cause neonatal epilepsy with late-onset episodic ataxia. *Journal of Neurology*, *263*, 334–343. https://doi.org/10.1007/s00415-015-7984-0

Untiet, V., Kovermann, P., Gerkau, N. J., Gensch, T., Rose, C. R., & Fahlke, C. (2017). Glutamate transporter-associated anion channels adjust intracellular chloride concentrations during glial maturation. *GLIA*, *65*, 388–400. https://doi.org/10.1002/glia.23098

de Vries, B., Mamsa, H., Stam, A. H., Wan, J., Bakker, S. L., Vanmolkot, K. R., & van den Maagdenberg, A. M. (2009). Episodic ataxia associated with EAAT1 mutation C186S affecting glutamate reuptake. *Archives of Neurology*, *66*, 97–101. https://doi.org/10.1001/archneurol.2008.535

Wadiche, J. I., Amara, S. G., & Kavanaugh, M. P. (1995). Ion fluxes associated with excitatory amino acid transport. *Neuron*, *15*, 721–728. https://doi.org/10.1016/0896-6273(95)90159-0

Winter, N., Kovermann, P., & Fahlke, C. (2012). A point mutation associated with episodic ataxia 6 increases glutamate transporter anion currents. *Brain*, *135*, 3416–3425. https://doi.org/10.1093/brain/aws255

Zerangue, N., & Kavanaugh, M. P. (1996). Flux coupling in a neuronal glutamate transporter. *Nature*, *383*, 634–637. https://doi.org/10.1038/383634a0

SUPPORTING INFORMATION

Additional supporting information may be found online in the Supporting Information section.

How to cite this article: Chivukula AS, Suslova M, Kortzak D, Kovermann P, Fahlke C. Functional consequences of *SLC1A3* mutations associated with episodic ataxia 6. *Human Mutation*. 2020;41:1892–1905. https://doi.org/10.1002/humu.24089